ChemPubSoc Europe

DOI: 10.1002/chem.201504983

CHEMISTRY A European Journal Communication

Electrochemistry

Pyrolysis of Animal Bones with Vitamin B12: A Facile Route to Efficient Transition Metal–Nitrogen–Carbon (TM-*N*-C) Electrocatalysts for Oxygen Reduction

Meiling Dou,[a] Duanpeng He,[a] Wenhao Shao,[a] Haijing Liu,[a] Feng Wang,*[a] and Liming Dai*[b]

Abstract: By pyrolyzing cattle bones, hierarchical porous carbon (HPC) networks with a high surface area (2520 $m^2 g^{-1}$) and connected pores were prepared at a low cost and large scale. Subsequent co-pyrolysis of HPC with vitamin B12 resulted in the formation of three-dimensional (3D) hierarchically structured porous cobalt–nitrogen–carbon (Co-*N*-HPC) electrocatalysts with a surface area as high as 859 $m^2 g^{-1}$ as well as a higher oxygen reduction reaction (ORR) electrocatalytic activity, better operation stability, and higher tolerance to methanol than the commercial Pt/C catalyst in alkaline electrolyte.

Platinum group metal catalysts have been widely used to promote the oxygen reduction reaction (ORR) in fuel cells.[1] However, the high cost and scarcity of noble-metal-based catalysts have precluded the fuel cell technology from commercial application. In this context, non-precious metal catalysts (NPMCs) have been extensively studied.[2] Although the amount of Pt needed for the desired catalytic effect could be reduced by using Pt alloys, commercial mass production of fuel cells would still require large amounts of Pt, and most NPMCs still cannot match Pt in catalytic performance.[1] Therefore, great efforts have been devoted to improving the activity and durability of NPMCs for ORR in fuel cells.[1] Currently, transition metal–nitrogen-doped carbon (TM-*N*-C, TM: Fe, Co, Cu, Ni, etc.) electrocatalysts are considered to be the most promising non-precious metal alternatives to the state-of-the-art platinum (Pt/C) electrocatalyst,[3] though their catalytic performance still needs to be further improved to meet the requirement for commercialization applications in fuel cells.

[a] *Dr. M. Dou, D. He, W. Shao, Dr. H. Liu, Prof. F. Wang*
State Key Laboratory of Chemical Resource Engineering, Beijing Key Laboratory of Electrochemical Process and Technology for Materials
Beijing University of Chemical Technology
Beijing 100029 (P.R. China)
E-mail: wangf@mail.buct.edu.cn

[b] *Prof. L. Dai*
Department of Macromolecular Science and Engineering
Case Western Reserve University
10900 Euclid Avenue, Cleveland, OH 44106 (USA)
E-mail: liming.dai@case.edu

Supporting information for this article is available on the WWW under http://dx.doi.org/10.1002/chem.201504983.

To improve the catalytic performance of TM-*N*-C catalysts, it is important to increase the ORR active sites (i.e., TM-N_x) and to enhance the mass transport of the electrolyte and reactant.[4] Because TM-N_x active sites formed during carbonization of the carbon precursor are mainly constrained in the sub 2 nm micropores,[5] the micropore distribution within the TM-*N*-C precursor plays an important role in increasing the active sites. On the other hand, a proper distribution of connected mesopores and macropores can also enhance the transport of the reactant/electrolyte towards or away from the active sites.[6] Therefore, it is highly desirable to synthesize TM-*N*-C catalysts with hierarchically controlled microstructures having a proper distribution of micropores, mesopores, and macropores. Unfortunately, most of the common carbon precursors (e.g., phenolic resin, furfural) used for the synthesis of many reported TM-*N*-C catalysts offer a rather limited control of the porous structure, and hence inefficient (TM-N_x) active site exposure, poor mass transport, and low ORR activity.[7] In contrast, three-dimensional (3D) carbon networks and foams could possess a high specific surface area, well-defined porosity with enhanced reactant/electrolyte diffusion, and excellent electrical and mechanical properties,[1] which should be useful for synthesizing highly active TM-*N*-C electrocatalysts toward ORR.

In addition, biotissues are natural and earth-abundant materials with well-defined hierarchical structures. In particular, animal bones having 3D ordered structures with apatite minerals sandwiched among the collagen fibrils are attractive as precursors for carbonization to produce hierarchically porous carbon (HPC) materials with a high specific surface area.[8] Here, the collagen fibrils could provide carbon and nitrogen sources required for the formation of N-doped HPCs while the robust apatite minerals would act as the hard template for porosity control. In the present study, we developed a co-carbonization approach to produce hierarchically structured cobalt and nitrogen co-doped porous carbon (Co-*N*-HPC) ORR electrocatalysts by pyrolyzing the Co-N_6 complex derived from vitamin B12 (VB12)[9] with the cattle bone-generated HPC. The resultant Co-*N*-HPC electrocatalysts were demonstrated to possess a surface area as high as 859 $m^2 g^{-1}$ and ORR electrochemical reactivity comparable or even better than that of commercial Pt/C electrode (20 wt% Pt, Johnson Matthey).

As schematically shown in Figure 1, we first synthesized HPC by carbonizing a piece of cattle bone at 400 °C for 3 h under argon atmosphere,[8c] followed by KOH-activation at 850 °C for 1 h and acid (2 M HNO_3)/deionized water (500 mL) washing to

© 2016 Wiley-VCH Verlag GmbH & Co. KGaA, Weinheim

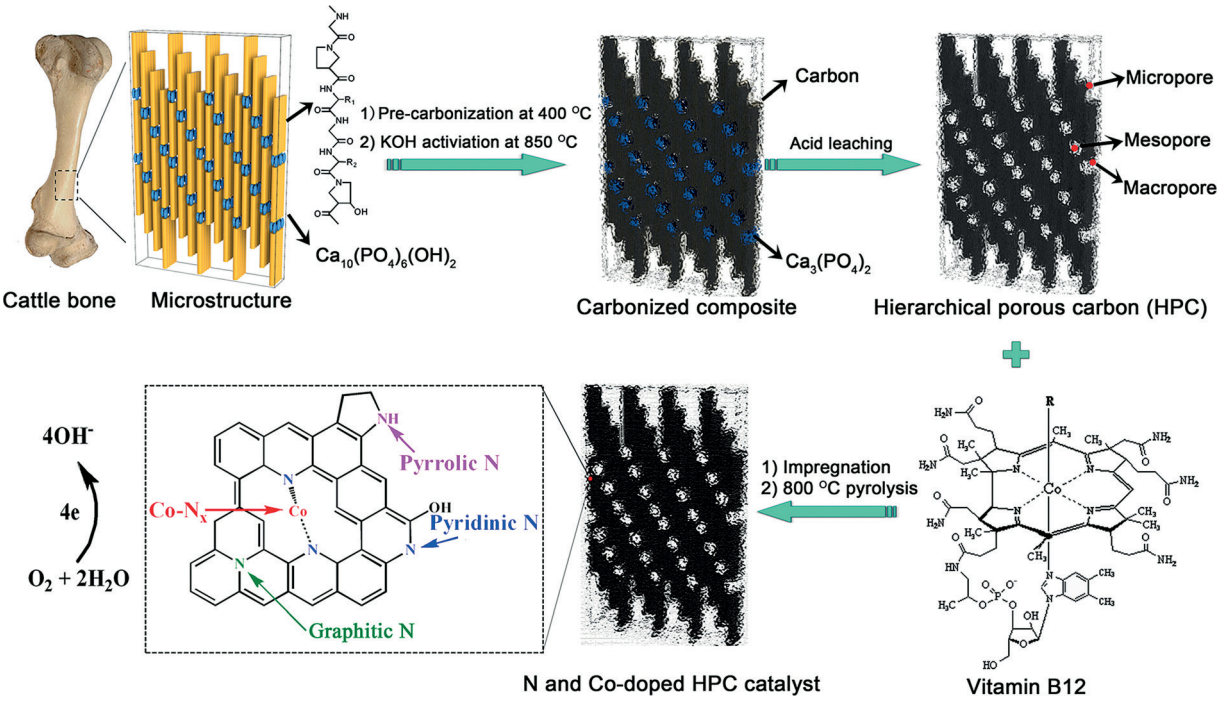

Figure 1. Schematic representation of procedures for the synthesis of Co-*N*-HPC.

remove the "hard template" of inorganic hydroxyapatite crystals. The Co-*N*-HPC electrocatalysts were then prepared by pyrolyzing the mixture of HPC and VB12 at 800 °C for 2 h in argon atmosphere. As reference, cobalt and nitrogen-doped carbon (Co-*N*-C) was fabricated by co-pyrolyzing commercial Vulcan XC-72 carbon black and VB12 under the same condition (see Figure 1). In addition, the VB12/HPC mass ratio optimization experiments (Figure S1 in the Supporting Information) revealed that the ORR activity increases when the VB12/HPC mass ratio rises from 0 to 1, with the best activity at VB12/HPC mass ratio of 1. However, the activity drops at a higher VB12/HPC mass ratio of 2.

The morphologies of HPC and Co-*N*-HPC were examined on a field-emission scanning electron microscope (FE-SEM, JEOL JSM-6701) and transmission electron microscope (TEM, JEOL JSM-2100). As seen in Figure 2a,c the HPC shows a 3D hierarchical honeycomb porous structure with interconnected pores containing open macropores (>50 nm) and channel mesopores (2–50 nm). After co-pyrolysis with VB12 (Figure 2b,d), the resulting Co-*N*-HPC still retains the hierarchical honeycomb porous framework characteristic of HPC. Besides, the TEM image of Co-*N*-HPC (Figure 2d) does not show any cobalt nitrate or cobalt oxide crystal, suggesting a complete pyrolysis of VB12 within the HPC. This is further supported by the XRD patterns for HPC and Co-*N*-HPC given in Figure S2 in the Supporting Information, which shows broad (002) and (100) peaks characteristic of partially crystalline carbon without any peak from cobalt nitrate or cobalt oxide crystals. The relatively low crystallinity with a high percentage of defects for HPC and Co-*N*-HPC are also evident in Raman spectra with a relatively high I_D/I_G ratio (Figure S3 in the Supporting Information).

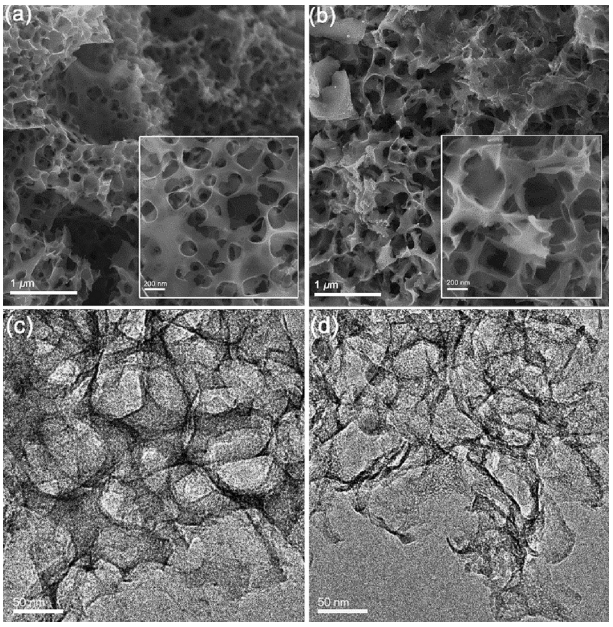

Figure 2. Typical SEM and TEM images of HPC (a, c) and Co-*N*-HPC (b, d). Scale bars: a) 1 μm, inset: 200 nm; b) 1 μm, inset: 200 nm; c) 50 nm; d) 50 nm.

The HPC and Co-*N*-HPC samples were further subjected to nitrogen adsorption measurements to determine the specific surface area and pore structure. As shown in Figure 3a,b both HPC and Co-*N*-HPC exhibit the type IV isotherm (according to IUPAC); a continuous increase in nitrogen adsorption with the pressure and an obvious hysteresis loop at high relative pressures. These results reveal the existence of hierarchical porous

© 2016 Wiley-VCH Verlag GmbH & Co. KGaA, Weinheim

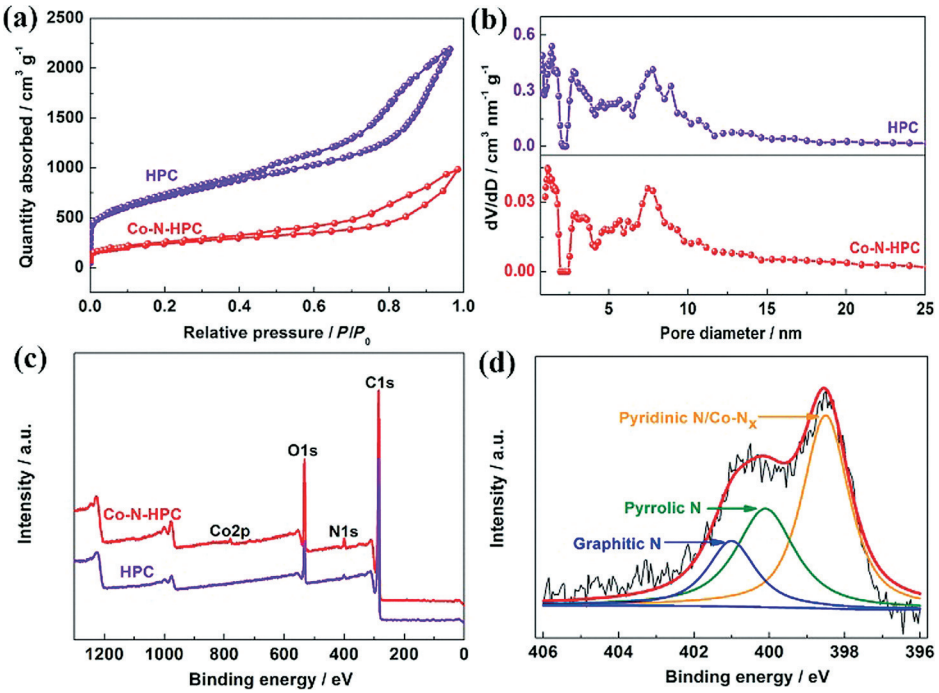

Figure 3. N_2 adsorption/desorption isotherm curves (a) and pore size distributions (b), XPS survey spectra of HPC and Co-*N*-HPC (c) and high-resolution N1s spectrum of Co-*N*-HPC (d).

structures of micropores, mesopores, and macropores.[13] Moreover, the BET surface area (S_{BET}) and pore volume were determined to be 2520 $m^2 g^{-1}$ and 3.18 $m^3 g^{-1}$, respectively, for HPC and 859 $m^2 g^{-1}$ and 1.37 $m^3 g^{-1}$ for Co-*N*-HPC. The significant decreases in the specific surface area and the pore volume observed for Co-*N*-HPC are probably due to partial blockage of the pores in HPC by decomposition products from the pyrolyzed VB12, as is the case for polyaniline-based TM-*N*-C[10] or bipyridine-based TM-*N*-C.[11]

To investigate chemical structures of HPC and Co-*N*-HPC, we performed the X-ray photoelectron spectroscopic (XPS) measurements. As seen in Figure 3c, the XPS survey spectrum of HPC shows the C1s, N1s, and O1s peaks with a relatively low N content of 1.57 at.%, presumably arising from the pyrolysis of collagen in the cattle bone. The corresponding XPS survey spectrum for Co-*N*-HPC shows the presence of 0.16 at.% Co and 2.38 at.% N with a N/Co atomic ratio of 14.87, which is consistent with the stoichiometric value of N/Co = 14 for VB12 in view of the additional N derived from the HPC (see Figure 1). This result indicates that the N atoms in the VB12 precursor have been efficiently utilized as the Co-N_x active sites (see Figure 3d) in Co-*N*-HPC with the easily accessible hierarchical porous structure. The high resolution XPS N1s spectrum in Figure 3d was deconvoluted into three components: graphitic N (401.2 eV), pyrrolic N (400.2 eV), and pyridinic N/Co-N_x (398.7 eV) (see also Figure S4 in the Supporting Information), respectively.[2b] The pyridinic N/Co-N_x is dominant, which is the main active site for ORR.[12] The graphitic N can incorporate in the conjugated carbon plane, resulting in a relatively high positive charge density on adjacent carbon atoms, where molecular oxygen is adsorbed to promote the ORR.[13] The XPS Co 2p3/2 spectrum (Figure S4 in the Supporting Information) can be deconvoluted into two peaks at binding energies of 781.6 eV and 779.7 eV, which were assigned to N- and O-coordinated Co, respectively.[4] The presence of the pronounced O1s peaks in Figure 3c is due to the incorporation of both chemically bonded (see Figure 1) and physically adsorbed oxygen.[14] The strong oxygen adsorption capability provides an additional advantage for the use of Co-*N*-HPC as ORR electrocatalysts.[15] Therefore, the combination of its unique surface chemistry with the 3D porous microstructure[16] could make the newly developed Co-*N*-HPC ideal electrocatalysts for ORR.

To evaluate the ORR activity, we first conducted cyclic voltammetry (CV) measurements on Co-*N*-HPC in N_2- and O_2-saturated 0.1 M KOH. For comparison, the Co-*N*-C and commercial Pt/C electrocatalysts were also examined under the same conditions. As expected, the double layer current increased with increasing S_{BET} in the order of HPC (2520 $m^2 g^{-1}$) > Co-*N*-HPC (S_{BET} = 859 $m^2 g^{-1}$) > Co-*N*-C (S_{BET} = 86 $m^2 g^{-1}$), (see Figure 4a). As expected, no redox current was observed for all of them in N_2-saturated 0.1 M KOH. Upon saturation of O_2 in the electrolyte, however, a cathodic respond between 0.7 and 0.8 V was observed, suggesting the occurrence of the ORR. Compared to Co-*N*-C, the Co-*N*-HPC electrode exhibited a more intensified ORR peak with a positive potential shift, indicating an improved ORR activity. This was further verified by the linear sweep voltammetry (LSV) curves measured on the rotating-disk electrode (RDE) at a rotating rate of 1600 rpm in O_2-saturated 0.1 M KOH (Figure 4b). As illustrated in Figure 4b, the Co-*N*-HPC exhibited a significantly enhanced ORR activity with a half-wave potential of 0.835 V, which is 40 and 8 mV higher than that of the Co-*N*-C and the commercial Pt/C electrode, re-

© 2016 Wiley-VCH Verlag GmbH & Co. KGaA, Weinheim

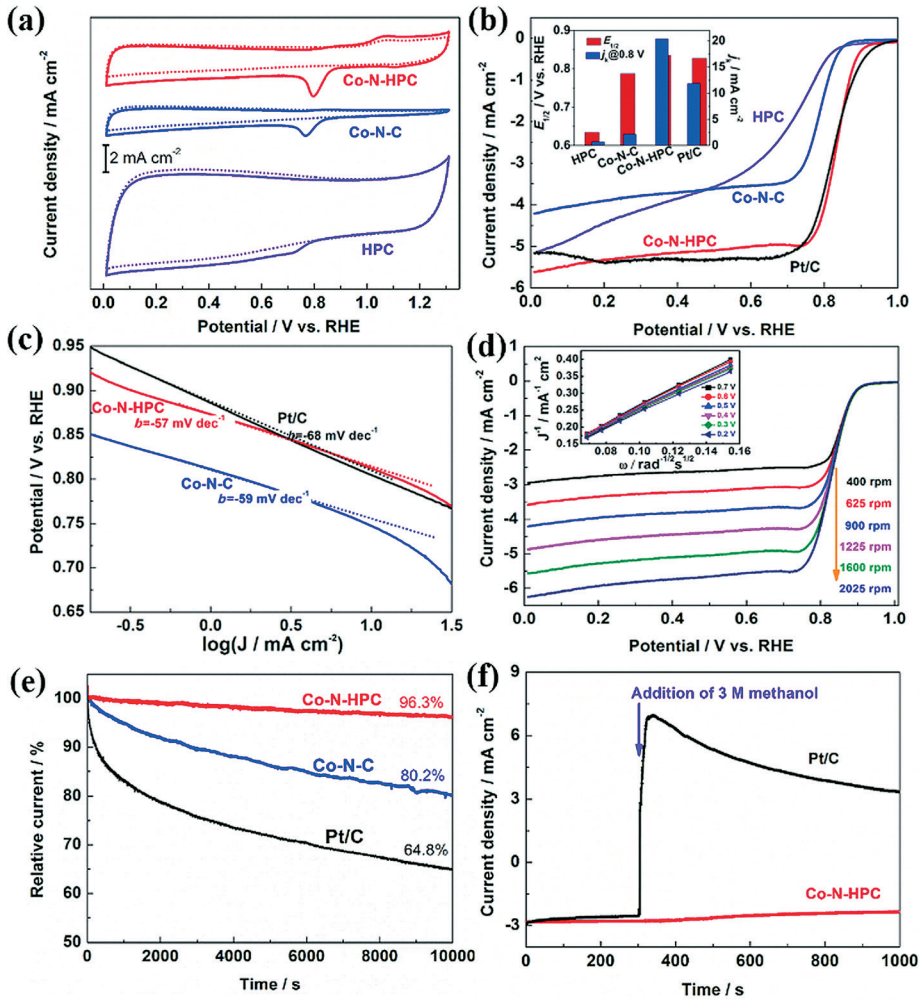

Figure 4. a) CV curves of HPC, Co-*N*-C, and Co-*N*-HPC in N_2- (dotted line) and O_2-saturated (solid line) 0.1 M KOH aqueous solution at the scan rate of 50 mV s^{-1}. b) LSV curves of the electrocatalysts in O_2-saturated 0.1 M KOH electrolyte at a scan rate of 5 mV s^{-1} and electrode rotation rate of 1600 rpm. Inset: summary of half-wave potentials and kinetic current densities at 0.8 V. c) Tafel plots and the corresponding slopes in high potential regions. d) LSV curves of Co-*N*-HPC at various rotating rates. Inset: the corresponding K-L plots. e) ORR chronoamperometric response of Co-*N*-HPC, Co-*N*-C, and Pt/C in O_2-saturated 0.1 M KOH aqueous solution at the electrode rotation rate of 900 rpm at 0.8 V. f) Chronoamperometric response of Co-*N*-HPC and Pt/C at 0.8 V in O_2-saturated 0.1 M KOH aqueous solution followed by addition of 3 M methanol.

spectively. The LSV curves in Figure 4b further show a high diffusion-limited current density of 5.2 mA cm^{-2} at 0.3 V for Co-*N*-HPC, which is about 1.4 times that of Co-*N*-C, suggesting an efficient transport path and sufficient accessible ORR active sites within the 3D porous Co-*N*-HPC electrode. The kinetic current density (j_k) of the Co-*N*-HPC was calculated to be 20.4 mA cm^{-2} at 0.8 V according to the Koutecky–Levich (K-L) equation,[17] which is almost ten-fold that of the corresponding value of the Co-*N*-C electrode and twice that of the Pt/C electrode, indicating, once again, that the Co-*N*-HPC electrocatalyst with Co-N_x ORR active sites embedded into the 3D porous carbon framework outperformed the commercial Pt/C electrode and silica templated mesoporous Co-*N*-C electrocatalysts.[4]

To further illustrate the unique structural advantages of Co-*N*-HPC, the Tafel curves were plotted in Figure 4c. The Tafel slope of the Co-*N*-HPC electrocatalyst was calculated to be 57 mV dec^{-1} in the low over-potential region, suggesting that the transfer of the first electron catalyzed by Co-*N*-HPC is probably the rate-determining step, similar to ORR catalyzed by Pt.[18] The Tafel slope increased in the order of Co-*N*-HPC (57 mV dec^{-1}) < Co-*N*-C (59 mV dec^{-1}) < Pt/C (68 mV dec^{-1}), implying that Co-*N*-HPC possesses improved ORR kinetics with the highest transfer coefficient for ORR due to the enhanced mass transport of the 3D porous carbon framework coupled with the embedded Co-N_x ORR active sites.[19] The transferred electron number involved in the ORR was calculated according to the K-L equation (Figure 4d) to be 3.87 for Co-*N*-HPC, which is higher than that of Co-*N*-C (3.45, Figure S5 in the Supporting Information), indicating that Co-*N*-HPC is more active and efficient towards ORR. The transferred electron number of Co-*N*-HPC (3.87) is close to that of the commercial Pt/C electrode (3.98, Figure S6 in the Supporting Information); both indicate an efficient four-electron oxygen reduction process.

Finally, the electrochemical stability was tested by chronoamperometric measurements in O_2-saturated 0.1 M KOH aqueous solutions at a constant voltage of 0.8 V. Figure 4e

© 2016 Wiley-VCH Verlag GmbH & Co. KGaA, Weinheim

shows almost no change (only 3.7% decrease) in the ORR current density for the Co-*N*-HPC electrode even after 10000 s operation, whereas the Co-*N*-C and Pt/C exhibited a 19.8% and 35.2% decrease, respectively, under the same condition. The Co-*N*-HPC electrocatalyst was further demonstrated to exhibit a superior fuel selectivity with only a slight deviation in the ORR current density upon the addition of 3 M methanol in the electrolyte, whereas a significantly increased methanol oxidation current was detected for the Pt/C electrode under the same condition. Clearly, therefore, the Co-*N*-HPC electrocatalyst possesses an excellent electrocatalytic activity, operation durability, and superb tolerance against methanol, promising for potential large-scale applications.

In summary, we have developed a facile, low-cost and scalable approach to 3D high-performance hierarchically structured ORR electrocatalysts by carbonizing cattle bones, followed by KOH-activation, acid (2 M HNO_3)/deionized water washing, and co-pyrolyzing with VB12. The Co-*N*-HPC electrocatalysts thus prepared were demonstrated to possess a 3D porous network structure with interconnected macropores, mesopores, and micropores of a high surface area for improved reactant/electrolyte transport and efficient ORR activity; these outperformed the commercial Pt/C electrode in not only catalytic activity but also operation stability and fuel selectivity. The methodology developed in this work is general in that it can be applied to the development of a large variety of high-performance TM-*N*-C electrocatalysts for various applications, including, but not limited to, fuel cells, batteries, and sensors.

Experimental Section

Synthesis: In a typical synthesis, the dried bone powder derived from cattle bone (purchased from market in Beijing) was pre-carbonized in a tubular furnace at 400 °C for 3 h under Ar atmosphere. Thereafter, the pre-carbonized product was ground and mixed with the active agent of KOH at a weight ratio of 1:1, then simultaneously activated and carbonized at 850 °C for 1 h under Ar atmosphere. The final product denoted as HPC was obtained after leaching in 2 M HNO_3, rinsing with distilled water, drying at 120 °C under vacuum. The cobalt and nitrogen-doped carbon electrocatalyst was then synthesized by pyrolyzing the mixture of Vitamin B12 (VB12) and HPC. In a typical experiment, 0.4 g VB12 and 0.4 g HPC were dispersed in 200 mL ethanol under stirring to yield a homogeneous solution, then the solvent was evaporated at 80 °C. The resultant product was calcined at 800 °C for 2 h in Ar atmosphere and denoted as Co-*N*-HPC. For comparison, Co-*N*-C electrocatalyst was also prepared using Vulcan XC-72 as carbon substrate and VB12 as cobalt and nitrogen sources.

Characterization: Field-emission scanning electron microscopy (FE-SEM) was taken on a JSM-6701 (JEOL) unit operating at 15 kV. Transmission electron microscopy (TEM) was carried out on a JSM-2100 (JEOL) unit operating at 200 kV. X-ray diffraction (XRD) measurements were performed on a Rigaku D/max-2500 diffractometer, using Cu K_α radiation ($\lambda = 1.54056$ Å) as the X-ray source. The nitrogen adsorption/desorption measurements were conducted on a Quantachrome AUTOSORB-SI instrument. The specific surface areas and pore size distribution were calculated by the Brunauer–Emmett–Teller (BET) and density functional theory (DFT) methods, respectively. Raman spectra were recorded with a Horiba Jobin Yvon LabRam HR800 confocal microscope using a laser of 632.8 nm to characterize the degree of graphitization of HPC and Co-*N*-HPC. The X-ray photoelectron spectrum (XPS) was profiled on the Thermo Fisher Scientific ESCALAB 250 using the C1s (284.6 eV) as the reference for binding energy calibration.

Electrochemical measurements: All electrochemical measurements, including cyclic voltammetry (CV), linear sweep voltammetry (LSV), and chronoamperometry, were performed on a computer-controlled ALS/DY2323 Bi-potentiostat workstation in a three-electrode cell at room temperature. The working electrode was prepared by pipetted 10 μL of homogeneous catalyst ink (10 mg Co-*N*-HPC or Co-*N*-C and100 μL of 5 wt.% Nafion solution were dispersed in 2 mL ethanol by sonication for 30 min) on a prepolished glassy carbon electrode (GCE, $d = 4$ mm), and dried at ambient condition. A saturated calomel electrode (SCE) and Pt wire were used as reference and counter electrode, respectively. The electrode loading of Co-*N*-HPC and Co-*N*-C are both 0.38 $mg_{cat}\,cm^{-2}$; the Pt loading of Pt/C is 0.023 $mg_{Pt}\,cm^{-2}$. All the potentials were calibrated in reference to the reversible hydrogen electrode (RHE).

Acknowledgements

This work was supported by National Natural Science Funds of China (51432003, 51125007).

Keywords: animal bones · cobalt-nitrogen-doped carbon · electrocatalyst · hierarchical pores · oxygen reduction reaction

[1] L. Dai, Y. Xue, L. Qu, H. J. Choi, J. B. Baek, *Chem. Rev.* **2015**, *115*, 4823.

[2] a) A. Morozan, B. Jousselme, S. Palacin, *Energy Environ. Sci.* **2011**, *4*, 1238; b) R. Silva, R. D. Voiry, M. Chhowalla, T. Asefa, *J. Am. Chem. Soc.* **2013**, *135*, 7823.

[3] a) J. Wang, H. Wu, D. Gao, S. Miao, G. Wang, X. Bao, *Nano Energy* **2015**, *13*, 387; b) G. Wu, C. M. Johnston, P. Zelenay, *Science* **2011**, *332*, 443; c) Y.-C. Wang, Y.-J. Lai, L. Song, Z.-Y. Zhou, J.-G. Liu, Q. Wang, X. D. Yang, C. Chen, W. Shi, Y.-P. Zheng, M. Rauf, S.-G. Sun, *Angew. Chem. Int. Ed.* **2015**, *54*, 9907; d) Y. Zhu, B. Zhang, X. Liu, D.-W. Wang, D. S. Su, *Angew. Chem. Int. Ed.* **2014**, *53*, 10673; *Angew. Chem.* **2014**, *126*, 10849; e) E. Proietti, F. Jaouen, M. Lefèvre, N. Larouche, J. Tian, J. Herranz, J. P. Dodelet, *Nat. Commun.* **2011**, *2*, 416.

[4] H.-W. Liang, W. Wei, Z.-S. Wu, X. Feng, K. Müllen, *J. Am. Chem. Soc.* **2013**, *135*, 16002; compared with the previously reported silica-templated mesoporous Co-*N*-C electrocatalysts (limiting diffusion current density at 0.3 V: 4.5 $mA\,cm^{-2}$ for VB12/Silica colloid; 3.9 $mA\,cm^{-2}$ for VB12/SBA-15; 3.7 $mA\,cm^{-2}$ for VB12/MMT),[4] our Co-*N*-HPC exhibited the highest diffusion-limited current density due clearly to the advantages associated with the 3D porous structure of a high specific surface area resulting from the simple pyrolysis of HPC with VB12 (see Figure 1).

[5] M. Lefevre, E. Proietti, F. Jaouen, J. P. Dodelet, *Science* **2009**, *324*, 71.

[6] a) D. W. Wang, F. Li, M. Liu, G. Q. Lu, H. M. Cheng, *Angew. Chem. Int. Ed.* **2008**, *47*, 373; *Angew. Chem.* **2008**, *120*, 379; b) H.-W Liang, S. Brüller, R. Dong, X. Feng, *Nat. Comm.* **2015**, *6*, 7992; c) H.-W. Liang, X. Zhuang, S. Brüller, X. Feng, *Nat. Comm.* **2014**, *5*, 4973.

[7] a) F. Jaouen, E. Proietti, M. Lefèvre, R. Chenitz, J.-P. Dodelet, G. Wu, H. T. Chung, C. M. Johnston, P. Zelenay, *Energy Environ. Sci.* **2011**, *4*, 114; b) Z. Li, G. Li, L. Jiang, J. Li, G. Sun, C. Xia, F. Li, *Angew. Chem. Int. Ed.* **2015**, *54*, 1494; *Angew. Chem.* **2015**, *127*, 1514.

[8] a) H. Liu, Y. Cao, F. Wang, Y. Huang, *ACS Appl. Mater. Interfaces* **2014**, *6*, 819; b) W. Huang, H. Zhang, Y. Huang, W. Wang, S. Wei, *Carbon* **2011**, *49*, 838; c) S. Wei, H. Zhang, Y. Huang, W. Wang, Y. Xia, Z. Yu, *Energy Environ. Sci.* **2011**, *4*, 736.

[9] S.-T. Chang, C.-H. Wang, H.-Y. Du, H.-C. Hsu, C.-M. Kang, C.-C. Chen, J. C. S. Wu, S.-C. Yen, W.-F. Huang, L.-C. Chen, M. C. Lin, K.-H. Chen, *Energy Environ. Sci.* **2012**, *5*, 5305.

© 2016 Wiley-VCH Verlag GmbH & Co. KGaA, Weinheim

[10] G. Wu, C. Johnston, N. H. Mack, K. Artyushkova, M. Ferrandon, M. Nelson, J. S. Lezama-Pacheco, S. D. Conradson, K. L. More, D. J. Myers, P. Zelenay, *J. Mater. Chem.* **2011**, *21*, 11392.
[11] R. Kothandaraman, V. Nallathambi, K. Artyushkova, S. C. Barton, *Appl. Catal. B* **2009**, *92*, 209.
[12] S. Maldonado, K. J. Stevenson, *J. Phys. Chem. B* **2005**, *109*, 4707.
[13] a) K. Gong, F. Du, Z. Xia, M. Durstock, L. Dai, *Science* **2009**, *323*, 760; b) H. Xiao, Z.-G. Shao, G. Zhang, Y. Gao, W. Lu, B. Yi, *Carbon* **2013**, *57*, 443.
[14] P. G. Collins, K. Bradley, M. Ishigami, A. Zettl, *Science* **2000**, *287*, 1801.
[15] S. Wang, L. Zhang, Z. Xia, A. Roy, D. W. Chang, J. B. Baek, L. Dai, *Angew. Chem. Int. Ed.* **2012**, *51*, 4209; *Angew. Chem.* **2012**, *124*, 4285.
[16] R. Ning, C. G, Q. Liu, J. Tian, A. M. Asiri, K. A. Alamry, C. M. Li, X. Sun, *Carbon* **2014**, *78*, 60.
[17] L. Geniès, R. Faure, R. Durand, *Electrochim. Acta* **1998**, *44*, 1317.
[18] Y. Li, W. Zhou, H. Wang, L. Xie, Y. Liang, F. Wei, J.-C. Idrobo, S. J. Pennycook, H. Dai, *Nat. Nanotechnol.* **2012**, *7*, 394.
[19] a) D. W. Banham, J. N. Soderberg, V. I. Birss, *J. Phys. Chem. C* **2009**, *113*, 10103; b) W. He, C. Jiang, J. Wang, L. Lu, *Angew. Chem. Int. Ed.* **2014**, *53*, 9503; *Angew. Chem.* **2014**, *126*, 9657; c) K. Elumeeva, J. Ren, M. Antonietti, T.-P. Fellinger, *ChemElectroChem* **2015**, *2*, 584.

Received: December 11, 2015
Published online on January 25, 2016

© 2016 Wiley-VCH Verlag GmbH & Co. KGaA, Weinheim